Structure of Poly(dialkylsiloxane) Melts: Comparisons of Wide-Angle X-ray Scattering, Molecular Dynamics Simulations, and Integral Equation Theory

Anton Habenschuss*

Oak Ridge National Laboratory, Oak Ridge, Tennessee 37831

Mesfin Tsige

Department of Physics, Southern Illinois University, Carbondale, Illinois 62901

John G. Curro

Department of Chemical & Nuclear Engineering, University of New Mexico, Albuquerque, New Mexico 87131

Gary S. Grest

Sandia National Laboratories, Albuquerque, New Mexico 87185

Shyamal K. Nath

CULGI Inc., Albuquerque, New Mexico 87131

Received January 26, 2007; Revised Manuscript Received May 29, 2007

ABSTRACT: Wide-angle X-ray scattering, molecular dynamics (MD) simulations, and integral equation theory are used to study the structure of poly(diethylsiloxane) (PDES), poly(ethylmethylsiloxane) (PEMS), and poly(dimethylsiloxane) (PDMS) melts. The structure functions of PDES, PEMS, and PDMS are similar, but systematic trends in the intermolecular packing are observed. The local intramolecular structure is extracted from the experimental structure functions. The bond distances and bond angles obtained, including the large Si−O−Si angle, are in good agreement with the explicit atom (EA) and united atom (UA) potentials used in the simulations and theory and from other sources. Very good agreement is found between the MD simulations using the EA potentials and the experimental scattering results. Good agreement is also found between the polymer reference interaction site model (PRISM theory) and the UA MD simulations. The intermolecular structure is examined experimentally using an appropriately weighted radial distribution function and with theory and simulation using intermolecular site/site pair correlation functions. Experiment, simulation, and theory show systematic increases in the chain/chain packing distances in the siloxanes as the number of sites in the pendant side chains is increased.

I. Introduction

The poly(dialkylsiloxanes) are a class of organo-silicon materials with properties of both commercial and theoretical interest because of their materials characteristics. This includes their outstanding resistance to aging and weathering, their ability to maintain good physical properties over a wide temperature range, their low surface tension, and their incompatibility with water and most organic materials.[1−4] Thus, they are used in many commercial applications such as lubricants, defoamers, greases, resins, adhesives, sealants, coatings, and relatively inert elastomers.[5,6] The poly(dialkylsiloxanes) differ from typical organic polymers in that the backbone consists of alternating Si and O atoms, with longer bond lengths than in carbon-based polymers. Unlike the carbon−carbon backbone of all-organic polymers, the −Si−O− backbone with virtually unhindered rotation makes for a very flexible polymer chain,[7] resulting in very low glass transition temperatures.

The purpose of this research is to measure the wide-angle X-ray scattering (WAXS) structure factor of PDES and PEMS and compare with molecular dynamics (MD) simulations and polymer reference interaction site (PRISM) theory. Together with the previously reported results[8] for PDMS, they can be compared to the intra- and intermolecular structure of previously studied polymers.[9−12] The structure and packing of the poly(dialkylsiloxanes) homopolymers, are also useful in the understanding of polymer blends of these materials.[13] From the experimental structure factors of the poly(dialkylsiloxanes), we can extract the short-range intramolecular order (i.e., the bond distances and bond angles) and the intermediate-range intermolecular packing in the liquid state. These results will then be compared to the simulations/calculations with the aim of improving the model parameters and also ascertaining the origin of the intermolecular order.

II. Experiment

Samples. PEMS and PDES were obtained in the form of clear viscous liquids at room temperature. The degree of tacticity of PEMS is not known, and only approximate molecular weights were provided. However, the structure as obtained from wide-angle diffraction experiments is typically not sensitive to molecular weight beyond chain lengths of a few tens of monomer repeat units, as discussed below. The known physical parameters of the PEMS and PDES samples are given in Table 1. All measurements were done at nominal room temperature.

* Corresponding author. E-mail: habenschussa@ornl.gov.

10.1021/ma0702290 CCC: $37.00
Published on Web 08/21/2007

Table 1. Properties of PEMS and PDES Used in Data Analysis

property	PEMS	PDES
sample source	Polymer Source, Inc. catalog # P2142-EMS	Scientific Polymer Products Inc. catalog # 981
physical state	clear, viscous liquid	clear, slightly viscous liquid
M_w	13000 g mol^{-1}	1500 g mol^{-1}
M_n	11500 g mol^{-1}	
no. of monomer repeat units	~135	15
polydispersity	1.13	
tacticity	unknown	NA
density, d	0.985 g cm^{-3} [a]	0.99 g cm^{-3} [b]
temp, T	298 K	298 K
site number density, ρ	0.03364 Å^{-3}	0.035004 Å^{-3}
absorption coefficient, μ	2.5034 cm^{-1}	2.2403 cm^{-1}
X-ray wavelength, λ	0.71069 Å	0.71069 Å

[a] Density taken as average of 0.98 g cm^{-3} (PDMS, melt) and 0.99 g cm^{-3} (PDES, crystal). [b] Crystal density from ref 43.

X-ray Scattering Experiments. The intensities were measured from the free, horizontal sample surface on a Scintag PAD-X $\theta-\theta$ diffractometer using reflection geometry.[14] Mo Kα radiation (λ = 0.7107 Å, 50 kV, 40 mA) and a solid-state detector were used. Intensities were measured over a momentum transfer range of $0.3 < k < 16$ Å^{-1}, where $k = 4\pi\lambda^{-1} \sin\theta$, with 2θ the scattering angle. The angular range was covered in five sections using slit sets of increasing divergence. The smaller divergence slits were used at low angles where the beam footprint must remain within the sample length and where higher angular resolution is needed for the sharper features at low angles. The larger slit sets were used for sections at increasing angles where resolution is less stringent and the greater irradiated volume compensates for the weaker intensities at higher angles. There was sufficient overlap between sections to allow normalization between sections. Sufficient counts were accumulated at each point to keep the statistical error in the k-weighted structure function (defined below) approximately uniform over the whole momentum transfer range. This entailed collecting well over 10^6 counts at the highest k values where the intensities are lowest.

III. Molecular Dynamics Simulations

The MD simulations were run using the LAMMPS parallel molecular dynamics code developed by Plimpton and coworkers[15] using both explicit atom (EA) and united atom (UA) potentials. A multiple time step second-order symplectic integrator (RESPA) was employed with an integration time step of 0.4 fs (2 fs) for the bond, 0.8 fs (4 fs) for the angle and torsion forces and 1.6 fs (8 fs) for the nonbonded van der Waals forces for the explicit atom (united atom) simulations. Isothermal calculations were carried out with a Nose-Hoover thermostat to simulate a canonical ensemble. The nonbonded potential is truncated and shifted at a cutoff of 12 Å for both the explicit and united atom potentials. For the case of the EA model, the MD simulations were first equilibrated for at least 6 ns, and then the atom positions were recorded every 2 ps for at approximately another 2 ns for further analysis. For the UA model, the simulations were first equilibrated for at least 6 ns; the positions of the CH_2 sites were saved every 20 ps for an additional 4 ns.

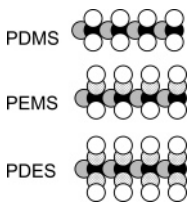

Figure 1. Schematic representation of the siloxanes studied. The gray circles are O atoms, the black circles are Si atoms, the open circles are CH_3 sites, and the dotted circles are CH_2 sites.

Chains of 20 monomer units with $-(CH_3)_3$ end groups were studied. Periodic boundary conditions were employed with 100 chains in each periodic box. Simulations were carried out for both explicit atom and united atom potentials. The explicit atom model employed was the class II potential developed by Sun and Rigby[16,17] and used previously in MD simulations on PDMS.[8,18] The PEMS was syndiotactic, and the densities used in the simulation were 0.986 g cm^{-3} for both PEMS and PDES.

The UA potential used here was an extension of the *hybrid united atom* potential developed by Frischknecht and Curro.[18] This united atom potential was developed for PDMS by matching the structure of the melt obtained from MD simulations using the class II explicit atom potential.[16,17] The bond stretching, bending, and torsional potentials have the form

$$V_b(r) = k_b(r - r_0)^2 \tag{1a}$$

$$V_a(\theta) = k_a(\theta - \theta_0)^2 \tag{1b}$$

$$V_t(\phi) = k_t[1 + \cos(n\phi)] \tag{1c}$$

where the trans state is defined to be at $\phi = 0°$. The intramolecular potential parameters for the hybrid united atom model are given in Table 2.

For the nonbonded potentials, the hybrid-UA model[18] employs both explicit atom and united atom potentials to model siloxanes. This feature somewhat complicates its use in standard MD codes. The Si and O atom interactions are taken directly from the established explicit-atom models[16,17] that have been

Table 2. United Atom Potentials[25]

bond	$k_b/2$ (kcal/(mol Å^2))	r_0 (Å)
Si−O	350.12	1.64
Si−CH_n	189.65	1.90
CH_n−CH_m	340.2	1.53
bending angle	**$k_\theta/2$ (kcal/(mol deg^2))**	**θ_0 (deg)**
Si−O−Si	14.14	146.46
O−Si−O	94.5	107.82
CH_n−Si−O	49.97	110.69
CH_n−Si−CH_m	49.97	109.24
CH_3−CH_2−Si	39.52	112.67

torsional angle	n	V_1 (kcal/mol)	V_2 (kcal/mol)	V_3 (kcal/mol)
Si−O−Si−O	1	−0.225	0	0
Si−O−Si−CH_n	3	0	0	−0.01
CH_3−CH_2−Si−O	3	0	0	−0.07
CH_3−CH_2−Si−CH_3	3	0	0	−0.07

Table 3. United Atom Nonbonded Potentials

site pairs	type	$\epsilon_{\alpha\gamma}$ (kcal/mol)	$\sigma_{\alpha\gamma}$ (Å)	$d_{\alpha\gamma}$ (Å)
Si−Si	9−6	0.131	4.29	3.53
Si−O	9−6	0.077	3.94	
Si−CH_3	12−6	0.160	3.72	3.57
O−O	9−6	0.080	3.30	2.63
O−CH_3	12−6	0.125	3.29	3.12
CH_3−CH_3	12−6	0.194	3.73	3.61
CH_2−CH_2	12−6	0.091	3.95	3.69
CH_2−Si	12−6	0.109	3.83	3.61
CH_2−CH_3	12−6	0.133	3.84	
CH_2−O	12−6	0.854	3.40	3.16

parametrized using a 9−6 potential. On the other hand, the CH_3 and CH_2 group interactions are united atom potentials using the more conventional 12−6 potentials. Thus, the potentials between Si and O atoms have the form

$$U_{\alpha\gamma}(r) = \epsilon_{\alpha\gamma}\left[2\left(\frac{\sigma_{\alpha\gamma}}{r}\right)^9 - 3\left(\frac{\sigma_{\alpha\gamma}}{r}\right)^6\right] \quad \alpha, \gamma = \text{Si, O} \quad (2a)$$

with the same mixing rules[16,17] as in the explicit atom potentials

$$\epsilon_{\alpha\gamma} = \frac{2\sigma_\alpha{}^3\sigma_\gamma{}^3\sqrt{\epsilon_\alpha\epsilon_\gamma}}{\sigma_\alpha{}^6 + \sigma_\gamma{}^6}, \quad \sigma_{\alpha\gamma} = \left(\frac{\sigma_\alpha{}^6 + \sigma_\gamma{}^6}{2}\right)^{1/6} \quad (2b)$$

All the other nonbonded pair interactions are taken to be of the 12−6 type

$$U_{\alpha\gamma}(r) = 4\epsilon_{\alpha\gamma}\left[\left(\frac{\sigma_{\alpha\gamma}}{r}\right)^{12} - \left(\frac{\sigma_{\alpha\gamma}}{r}\right)^6\right] \quad (3a)$$

with the mixing rules[18]

$$\epsilon_{\alpha\gamma} = \sqrt{\epsilon_\alpha\epsilon_\gamma}, \quad d_{\alpha\gamma} = (d_\alpha + d_\gamma)/2 \quad (3b)$$

where d is the effective hard-core diameter defined according to[19,20]

$$d = \int_0^\infty \{1 - \exp[-U^{\text{rep}}(r)/k_BT]\} \quad (4)$$

The formulation of the mixing rules in eq 3b in terms of the hard-core diameters (rather than the Lennard-Jones σ parameter) permits it to be used to describe cross-interactions between Si or O atoms and the united atom CH_3 and CH_2 sites. In eq 4 $U^{\text{rep}}(r)$ is the repulsive part of the potential in eqs 2 or 3 and is defined in the next section. All the nonbonded, UA parameters used in our MD simulations are given in Table 3.

Recently, Makrodimitri, Dohrn, and Economou[21] performed MD simulations of PDMS with a different UA model, and comparisons were made with the hybrid UA model used here. In addition, these authors used simulation to estimate the solubility of alkanes and gases in the PDMS.

IV. PRISM Theory

The polymer interaction site model or PRISM theory is an integral equation theory developed by Curro and Schweizer[22−24] as an extension of the RISM theory of Chandler and Andersen.[25,26] PRISM theory has been discussed in detail in previous reviews[27] and will only be described briefly here.

PRISM theory represents the polymer chains as a collection of overlapping interaction sites as seen in Figure 1 for the silicone macromolecules PDMS, PEMS, and PDES. We assume that the polymers are sufficiently long so that end effects can be neglected[24] and that all monomers along the chain backbone are equivalent. For PEMS the chain was taken as isotactic, and the densities used were 0.99 g cm^{-3} for both PEMS and PDES.

PRISM theory is a theory for the structure of the polymer which is characterized by the intermolecular pair correlation functions $g_{\alpha\gamma}(r)$ between sites making up the monomers on different chains.

$$g_{\alpha\gamma}(r) = \int \frac{\langle\rho_\alpha(r')\,\rho_\gamma(r+r')\rangle}{\rho_\alpha\rho_\gamma}\,\mathrm{d}r' \quad (5)$$

The theory makes use of the generalized Ornstein−Zernike equation[27−29] of Chandler and Andersen.

$$\hat{\mathbf{H}}(k) = \hat{\mathbf{W}}(k)\cdot\hat{\mathbf{C}}(k)\cdot[\hat{\mathbf{W}}(k) + \hat{\mathbf{H}}(k)] \quad (6)$$

In eq 6 carets denote Fourier transformation with wave vector k. The average intermolecular packing and intramolecular structure are characterized by $H_{\alpha\gamma}(r) = g_{\alpha\gamma}(r) - 1$ and $\Omega_{\alpha\gamma}(r)$, respectively.

$$\hat{\Omega}_{\alpha\gamma}(k) = \frac{1}{N}\sum_{i\in\alpha,\, j\in\gamma}^{N}\left\langle\frac{\sin kr_{ij}}{kr_{ij}}\right\rangle \quad (7)$$

The summation in eq 7 is over intramolecular pairs of sites on a single chain, having N monomers. The Greek letters α or γ refer to the various site types Si, O, CH_2, and CH_3 making up the various monomer units in the silicones depicted in Figure 1.

The generalized Ornstein−Zernike equation can be viewed as a definition for the intermolecular direct correlation function[25−27] $C_{\alpha\gamma}(r)$. Since $C_{\alpha\gamma}(r)$ is a short-range function of r, we employ the well-known Percus−Yevick (PY) approximate closure from the theory of atomic liquids[19,27]

$$C_{\alpha\gamma}(r) \cong \{1 - \exp[\beta U_{\alpha\gamma}(r)]\}[H_{\alpha\gamma}(r) + 1] \quad (8)$$

where $U_{\alpha\gamma}(r)$ is the nonbonded potential. Equation 8 can be used to eliminate the direct correlation function from eq 6, thus providing a relationship between the intermolecular packing $g_{\alpha\gamma}(r)$ and intramolecular structure $\Omega_{\alpha\gamma}(r)$ of the polymer liquid. For atomic liquids[19] and polymer melts[27] at liquidlike densities the liquid structure is primarily determined from the repulsive part of the potential. Consequently, we follow Weeks, Chandler, and Andersen[20] by dividing the total nonbonded potential into a repulsive part

$$U_{\alpha\gamma}^{\text{rep}}(r) = U_{\alpha\gamma}(r) + \epsilon, \quad r \le r^*$$
$$U_{\alpha\gamma}^{\text{rep}}(r) = 0, \quad r \ge r^* \quad (9a)$$

and an attractive or perturbative contribution $U_{\alpha\gamma}^{\text{att}}(r)$.

$$U_{\alpha\gamma}^{\text{att}}(r) = -\epsilon_{\alpha\gamma}, \quad r \le r^*$$
$$U_{\alpha\gamma}^{\text{att}}(r) = U_{\alpha\gamma}, \quad r \ge r^* \quad (9b)$$

In eqs 9 $U_{\alpha\gamma}(r)$ is the total UA potential from either eq 2 or eq 3, $\epsilon_{\alpha\gamma}$ is the depth of the potential well, and r^* is the location of the potential minimum (σ and $2^{1/6}\sigma$ for the 9/6 and 12/6 potentials). In this work we use only the repulsive part of the potential in the closure relation. The PRISM theory outlined here has been applied previously to polyolefin[28] and PDMS[8,29] melts. For the present application to silicones, each monomer contains 6 (PDES) or 5 (PEMS) independent united atom sites representing O, Si, CH_2, and CH_3 moieties.

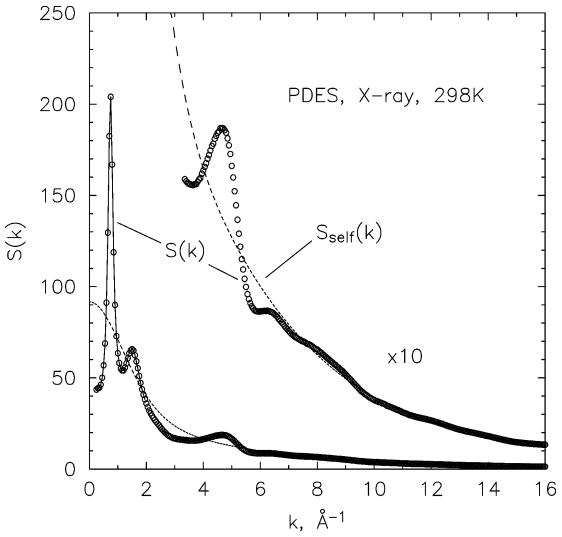

Figure 2. Static coherent scattering function $S(k)$ and the self-scattering $S_{self}(k)$ from uncorrelated, independent scattering sites in PDES.

For a given intramolecular structure function $\hat{\Omega}_{\alpha\gamma}(k)$, eqs 6 and 8 can be solved numerically for the intermolecular radial distribution functions. One could make use of Flory's ideality hypothesis[30] by approximating the single chain structure in a polymer melt as a chain without long-range excluded-volume interactions. More exact calculations on flexible chains, however, require that the intramolecular structure be determined self-consistently with the intermolecular packing. This self-consistent computation proceeds by replacing the full many chain computation with a single chain Monte Carlo simulation in the potential energy field

$$U(\mathbf{R}) = U_E + W(\mathbf{R}) \tag{10}$$

where U_E represents the conventional bonded and nonbonded interactions that an isolated chain would experience. $W(\mathbf{R})$ is a medium-induced potential that mimics the effects of the other chains in the system. The essence of the Flory hypothesis[30] is that the repulsive excluded-volume interactions and attractive medium-induced potentials effectively cancel each other out in eq 10. In this work we approximate this medium-induced potential as being pairwise additive with the form[27,31,32]

$$\beta\hat{W}_{\alpha\gamma}(k) = -\sum_{i,j}\hat{C}_{\alpha i}(k)\,\hat{S}_{ij}(k)\,\hat{C}_{j\gamma}(k) \tag{11}$$

where the partial structure factors are defined as

$$\hat{S}_{\alpha\gamma}(k) = \rho_\alpha\hat{\Omega}_{\alpha\gamma}(k) + \hat{H}_{\alpha\gamma}(k) \tag{12}$$

Since the medium-induced potential depends on the intermolecular direct correlation functions and vice versa, it is necessary to solve the self-consistent problem iteratively. We use a Picard iteration procedure that has been described previously.[28] It is important to note that reweighting techniques can be employed so that the Monte Carlo simulation does not have to be repeated in each iteration.[28]

V. Results and Discussion

The five individual regions of X-ray scattering data were corrected for polarization[33] and scattering volume dependent absorption[34] and then combined using the overlapping regions. The combined intensity curve was then corrected for monochromator discrimination,[35] incoherent scattering,[36] and multiple scattering.[37] The corrected intensity curve in arbitrary units was

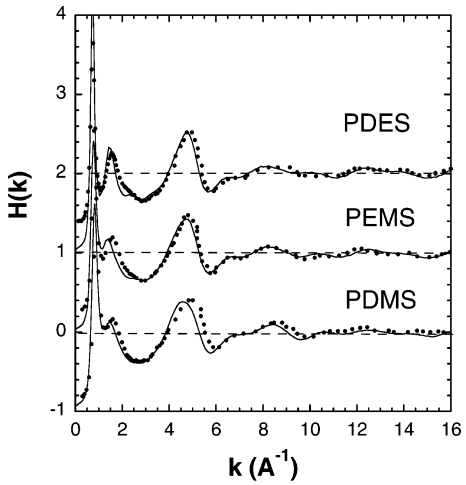

Figure 3. Total structure function $H(k)$ for PDES, PEMS, and PDMS. The points are the experimental data, and the lines are the MD simulations using the EA potential. The results for each siloxane are shifted vertically for clarity. The points at wave vectors below about 0.5 Å^{-1} are less accurate due to experimental uncertainties at low scattering angles.

then normalized to the self-scattering from uncorrelated scattering sites, $S_{self}(k)$

$$S_{self}(k) = \sum_{i=1}^{n} x_i b_i^2(k) \tag{13}$$

where n is the number of sites within a repeat unit, and x_i and $b_i(k)$ are the mole fraction and coherent scattering factors, respectively, of the sites. The coherent scattering factors for Si and O were taken from the *International Tables for X-Ray Crystallography*.[38] For CH_2 and CH_3, we used group scattering factors[39] which treat CH_2 and CH_3 as united atom sites. The resulting normalized static coherent scattering function $S(k)$ and the self-scattering $S_{self}(k)$ for PDES at 25 °C are shown in Figure 2.

The structure factor $H(k)$, containing the structurally sensitive part of the data, is defined[39] as

$$H(k) = M(k)[S(k) - S_{self}(k)] \tag{14}$$

where the modification function $M(k)$ is given by

$$M(k) = \left[\sum_{i=1}^{n} x_i b_i(k)\right]^{-2} \tag{15}$$

The total structure factor for PEMS and PDES is shown in Figure 3, together with the previous experimental results[8] for PDMS. Also shown in this figure are the MD simulations for all three siloxanes obtained using the EA potentials. Although not shown in the figure, the MD simulations resulting from the UA potentials are almost identical to the EA potential results at high wave vectors. It can be seen from Figure 3 that the agreement between the X-ray scattering experiments and MD simulations is very good, particularly at high wave vectors. At wave vectors greater than ~4 Å^{-1} the structure function $H(k)$ is primarily determined by the intramolecular conformations of the macromolecules. Hence, the agreement between experiment and MD indicates that the intramolecular components of both the EA and the hybrid UA potentials are accurate for siloxanes. This is confirmed by comparing Tables 2 and 4, where it can be observed that the bond distances and bond angles extracted

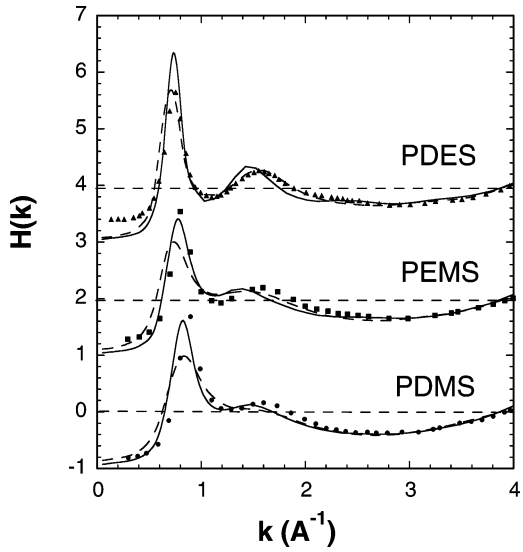

Figure 4. Low-k total structure function $H(k)$ for PDES, PEMS, and PDMS. The points are the experimental data, the solid lines are the MD simulations using the EA potential, and the dashed lines are the MD simulations using the UA potential. The results for each siloxane are shifted vertically for clarity. The points at wave vectors below about 0.5 Å^{-1} are less accurate due to experimental uncertainties at low scattering angles

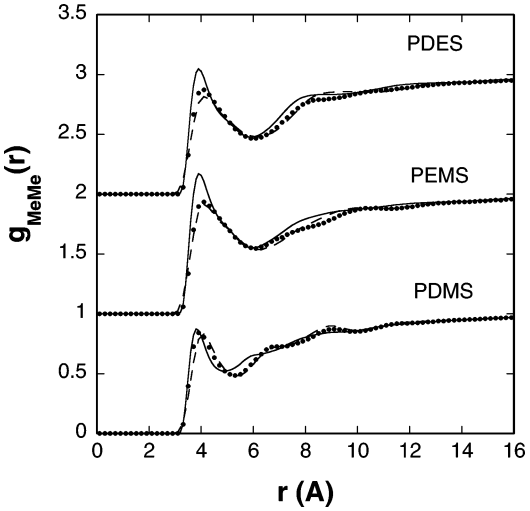

Figure 5. Intermolecular radial distribution functions between methyl groups. The solid curves are from PRISM theory, the points are from the MD simulations using the UA potential, and the dashed curves are from the MD simulations using the EA model. The results for each siloxane are shifted vertically for clarity.

from the X-ray scattering (discussed below) are in good agreement with the corresponding values in the UA potential.

At low wave vectors the total structure factor $H(k)$ contains information on both intramolecular and intermolecular structure. The intermolecular contribution to $H(k)$ arises from correlations between sites on *different* chains and contains information on chain−chain packing in the polymer melt. A prominent peak near $k \sim 1$ Å^{-1} occurs in all the siloxanes and is due to a balance between intermolecular and intramolecular effects. To focus on the intermolecular packing, we plotted the low-k structure factors from scattering in Figure 4, along with the MD simulation results from both the EA and UA potentials. Note that the location of the low angle peak shifts to lower wave vectors as we proceed from PDMS to PDES. This suggests that additional bulkiness in the pendant side chains tends to force the siloxane backbones to be farther apart on the average as will be discussed later.

It can be seen that the EA simulations are in excellent agreement with the scattering for PEMS and PDMS, whereas the UA simulations slightly underestimate the intensity of the low angle peak. Note also that both the EA and UA MD $H(k)$ results are lower than experiment below wave vectors $k \leq 0.5$ Å^{-1} for PDES and PEMS. It should be pointed out that the X-ray scattering measurements are not accurate in this low angle wave vector range. Hence, the EA simulations are probably more accurate than the actual experimental results below $k \leq 0.5$ Å^{-1}. Clearly all three siloxanes must have approximately the same value of $H(0)$ in the zero wave vector limit since the compressibilities would be expected to be very close for PDES, PEMS, and PDMS.

The experimental structure factor provides valuable information about the *average* intramolecular conformations and intermolecular packing of the siloxane melts. The simulations and PRISM theory are capable of giving more detailed information about the way individual atoms pack in the liquid state through the individual site/site correlation functions $g_{\alpha\gamma}(r)$. There are 6 (PDMS), 15 (PEMS), and 10 (PDES) independent pair correlation functions that characterize the intermolecular packing of the various siloxanes. In Figure 5, we show the intermolecular radial distribution functions $g_{\mathrm{MeMe}}(r)$ between methyl species obtained from PRISM theory and from MD simulations using both the EA and UA potentials. It can be seen that PRISM theory and the UA simulations, both of which used the same site/site potentials, are in reasonably good agreement. Moreover, the EA and UA simulations are also in good agreement. Note that $g_{\mathrm{MeMe}}(r)$ has a prominent peak located at ∼4.0 Å for all three siloxanes. This indicates that in the liquid the CH_3 groups, on the average, are almost in contact. From Table 3 we note that the effective hard-core diameter between methyl groups is $d = 3.61$ Å.

By contrast, we expect that the correlations between atoms on the siloxane backbone chains will be screened due to the presence of the pendant side-chain sites. This is clearly seen in Figure 6 for the intermolecular radial distribution function $g_{\mathrm{OO}}(r)$ between oxygen atoms. The effective hard-core distance between oxygen atoms is 2.63 Å (see Table 3). It can be seen from Figure 6 that the pair correlation functions are essentially

Table 4. Short-Range Intramolecular Structure for Some Poly(dialkylsiloxanes) from X-ray Diffraction

	r (Å)			bending angle, deg		
intramolecular correlations	PDMS[a]	PEMS	PDES	PDMS[a]	PEMS	PDES
Si−O	1.63	1.64	1.64			
Si−C[b]	1.84	1.86	1.88			
C−C		1.54[c]	1.54[c]			
Si−(O)−Si	3.14	3.16	3.17	150	150	150
O−(Si)−O	2.60	2.60	2.60	106	105	105
C−(Si)−C	3.00	3.04	3.07		109.5[d]	
O−(Si)−C	2.84	2.88	2.90	110	111	111
Si−(C)−C		2.82	2.84		112.0[c,d]	112.0[c,d]

[a] From ref 8. [b] C represents either a CH_2 or CH_3 united atom site. [c] From ref 41. [d] Fixed.

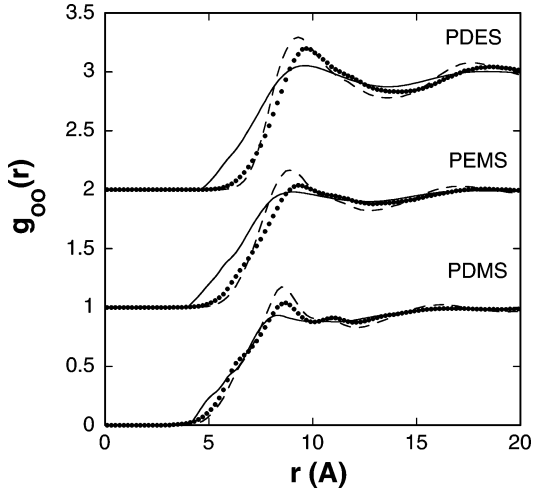

Figure 6. Intermolecular radial distribution functions between oxygen atoms. The solid curves are from PRISM theory, the points are from the MD simulations using the UA potential, and the dashed curves are from the MD simulations using the EA model. The results for each siloxane are shifted vertically for clarity.

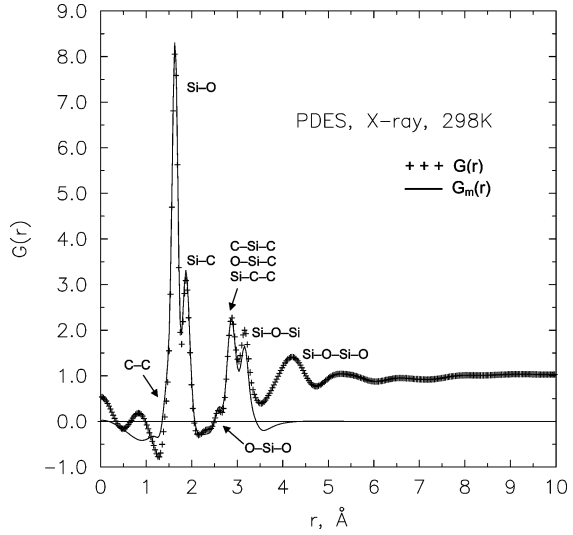

Figure 7. Total radial distribution function, $G(r)$, compared to the partial intramolecular model $G_m(r)$ for PDES. Some of the short-range intramolecular structural features are indicated in the figure.

zero for OO separations of less than ~5 Å; hence, the oxygen atoms are never in direct contact. The average packing distances between oxygen atoms, as indicated by the peak positions of $g_{OO}(r)$, are much larger and system dependent: 8.6 Å (PDMS), 9.2 Å (PEMS), and 9.6 Å (PDES). The agreement between PRISM theory and both the UA and EA MD simulations is about as expected on the basis of previous studies on polyolefins.[28] Generally PRISM theory is somewhat less accurate in predicting correlations between sites that are highly screened.[27] This likely is due to the use of the atomic PY closure for the direct correlation function in eq 8 which does not accurately account for the close proximity of intramolecular sites. This effect is also seen in the RISM theory of small molecule liquids.[26]

It is possible to extract an average radial distribution function from the experimental X-ray scattering data. The intramolecular structural contribution to $H(k)$ consists of correlations between sites within the *same* polymer chain, specified by bond distances, bond angles, and torsional rotations. Typically, only correlations among the first few nearest neighbors within a chain contribute identifiable features to total structure factor. The region of the total structure factor above $k = 4$ Å^{-1} is dominated by these intramolecular correlations. Since the intermolecular contributions quickly damp out beyond $k = 4$ Å^{-1}, we can use the procedure discussed previously[8] to extract a partial intramolecular structure factor $H_m(k)$ describing bond distances and bond angles in PEMS and PDES by a least-squares method from the high-k part of the total structure factor. The results are given in Table 4, where the previously derived[8] values for PDMS are also listed.

To analyze the experimental intermolecular structural information, we construct the total radial distribution function

$$G(r) = 1 + (2\pi^2\rho r)^{-1}\int_0^\infty kH(k)\sin(kr)\,dk \qquad (16)$$

where ρ is the site number density given in Table 1. To avoid truncation errors in the Fourier transform in eq 16, we followed the previously described method for extending $H(k)$ to high momentum transfer values.[8] The total $G(r)$ for PDES is shown in Figure 7, together with $G_m(r)$, the Fourier transform of the partial intramolecular structure factor $H_m(k)$ obtained above.

The total structure functions shown in Figure 3 indicate that the structures of PDMS, PEMS, and PEDS are very similar. However, systematic differences do exist as can be seen in the experiments and simulations in Figure 4. There are sharp "intermolecular" peaks at 0.875, 0.80, and 0.75 Å^{-1} for PDMS, PEMS, and PDES, respectively. Further differences occur in the peaks at 1.6 and 4.8 Å^{-1} as well as in the minimum near 2.9 Å^{-1}. Real differences in the "intramolecular region" at high momentum transfers also exist but are not discernible at the scale in Figure 3. These reflect mainly the different local intramolecular architecture in PDES, PEMS, and PDMS, i.e., the replacement of one or both of the methyl groups with ethyl groups.

The structure functions beyond about $k = 4$ Å^{-1} are largely due to the intramolecular structure, especially the first few near-neighbor sites within the chain. The bond lengths and bond angles obtained from the experimental structure functions above ~4 Å^{-1} are given in Table 4. No significant differences in the local intramolecular parameters are found for these materials. The average Si−O bond distance of 1.64 Å can be compared to the mean value of 1.622(14) Å from 70 instances of Si−O bonds in crystalline organo-silicon compounds.[40] Similarly, the average Si−C bond length of 1.86 Å in Table 2 agrees with the mean value of 1.857(18) Å based on 552 samples of Si−C bonds in crystal structures in the literature.[40]

In determining the bending angles in Table 4, the C−C bond distance and the Si−C−C and C−Si−C bond angles were fixed at known values[41] in the least-squares analysis. Furthermore, 2-fold symmetry was assumed around the Si site. The bond angle for Si−O−Si of 150° is slightly larger than, and the bond angle for O−Si−O of 105° is slightly smaller than, the previously reported values.[41] However, the large Si−O−Si bond angle is confirmed in these polymer melts.

The features in the radial distribution function shown in Figure 7 are mostly attributable to the above intramolecular structure. To observe the intermolecular correlations, the high-r region of $G(r)$ is emphasized in Figure 8, where the r^2-weighted $G(r)$ is shown to 40 Å. For comparison, the same functions for poly(ethylene) (PE) and poly(isobutylene) (PIB) are also shown. It is clear that the $G(r)$ are nontrivial to long distances, with regular periodic oscillations (beyond the short-range structure). They consist of site density oscillations reminiscent of the $G(r)$ of hard-sphere fluids, where they are due to correlations between an origin site and nearest-neighbor sites, next-nearest-neighbor sites, etc. A similar interpretation of the $G(r)$ for the polymers

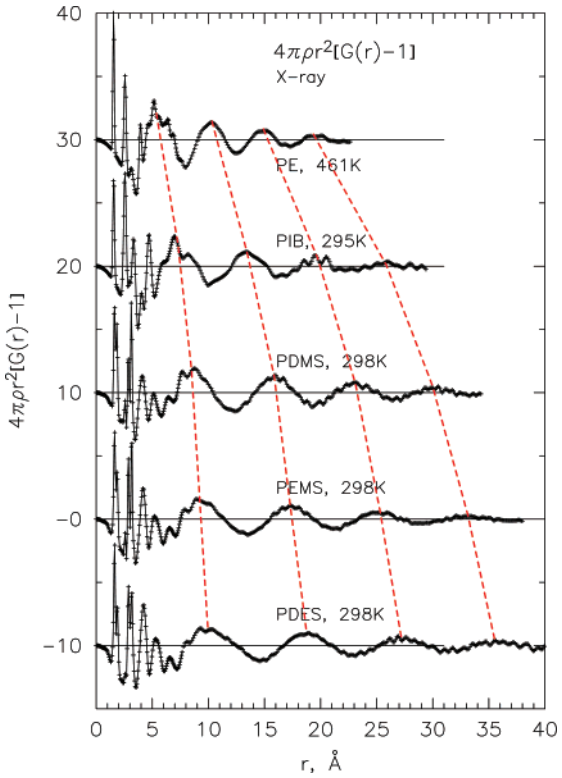

Figure 8. r^2-weighted total radial distribution function extracted from scattering data, $G(r)$, for PE, PIB, PDMS, PEMS, and PDES. The results for each polymer are shifted vertically for clarity. The small, high-frequency oscillations superimposed on the r^2-weighted correlations are numerical artifacts in taking the Fourier transforms. The dashed lines are guides to the eye in comparing the chain−chain correlations of each polymer.

shown in Figure 8 can be made: i.e., the oscillations in the $G(r)$ are simply the correlations between chains taken as flexible cylinders of some averaged diameter dependent on the chain architecture. The first big peak is simply the average chain−chain distance at contact. This occurs near 5 Å for PE and near 8−10 Å for the poly(dialkylsiloxanes). And since these are condensed fluids, where the chains are in repulsive contact, these values are an approximate measure of the average chain diameter. This interpretation agrees with the chain architecture of the polymers shown, where we have increasing site diameters (C to Si) and an increasing number and size of pendant groups (from none in PE to methyl and ethyl groups in PIB and the poly(dialkylsiloxanes)), which indicates increasing average chain diameters. This view ignores the local architecture of the chains and the details of the interactions between individual sites between chains but views each chain as a flexible cylinder of an average diameter determined by the size and number of substituent groups. Similarly, the second, third, etc., peaks in the $G(r)$ are simply chain−chain correlations from the next-nearest neighbors and further removed neighbors. It is curious that these correlations persist to about the fourth nearest-neighbor chains in each of the polymers. These intermolecular correlations can persist to 40 Å in the case of PDES. Note the small, high-frequency oscillations superimposed throughout the correlation functions in Figure 8. These are numerical artifacts introduced when the inverse Fourier transform is taken in eq 16.

The $G(r)$ function extracted from scattering data is primarily a (b_i-weighted) collective average of all the various site/site pair correlation functions. In addition, it contains some residual intramolecular contributions. In principle, $G(r)$ could be computed from the simulations and theory. However, since $G(r)$ is a measure of chain−chain correlations, it is instructive to examine the intermolecular radial distributions from theory and simulation between the backbone sites O and Si. The OO pair correlation functions for the three siloxanes are shown in Figure 6. In Figure 9, we display the r^2-weighted SiSi intermolecular radial distributions of the various siloxanes obtained from PRISM theory and the MD simulations. As in the case of the experimental data in Figure 8, the SiSi correlation functions from theory and simulation exhibit long-range oscillations with a period that increases with the size of the pendant groups attached to the siloxane backbones. In addition, the positions of the first two peaks for the siloxanes in Figure 9 are in approximate agreement with the corresponding experimental peaks in Figure 8. Such agreement reinforces the interpretation of $G(r)$ as a measure of chain thickness.

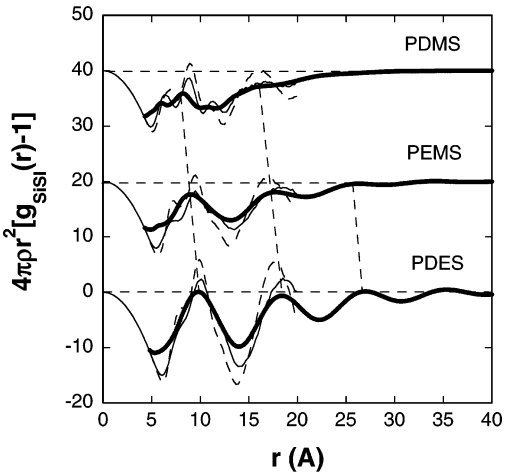

Figure 9. r^2-weighted intermolecular radial distribution functions between Si atoms for PDMS, PEMS, and PDES. The thick solid curves are from PRISM theory, the thin solid curves are from MD simulations using the UA potential, and the dashed curves are from MD simulations using the EA potential (compare to Figure 8). The results for each polymer are shifted vertically for clarity. The dashed lines are guides to the eye in comparing the structural features of each polymer.

This simple interpretation of the $G(r)$ implies that these siloxanes do not form persistent higher order structures in the melt. Such is not always the case. Some vinyl polymers, such as *i*-poly(propylene), *i*-poly(1-butene), *i*-poly(4-methyl-1-pentene), and poly(styrene), have nontrivial behavior[9] of the $G(r)$. These are interpreted as arising from a secondary structure, namely correlations between helical regions, driven by steric constraints from the side groups. Such steric effects apparently do not drive the structure into persistent helical regions in the poly(dialkylsiloxane) melts, presumably because of the longer Si−C and Si−O bond lengths and the flexibility of the Si−O−Si linkage. Note that the $G(r)$ in Figure 8 for the three siloxanes show systematic behavior with no anomaly for PDES, which has a very low molecular weight. This is consistent with earlier results for alkanes of various molecular weights,[41] which show that the intermediate-range structure becomes independent of chain length beyond 10 repeat units.

VI. Conclusions

Wide-angle X-ray scattering experiments, together with MD simulations and PRISM theory, were employed to study the packing and structure of PDMS, PEMS, and PDES silicone melts. Systematic differences in the intermolecular chain packing were observed due to screening of the siloxane backbones by the pendant methylene and methyl groups. The average distance

between chains increased monotonically (see Figure 8) as the number of sites on the pendant chains increased: 8.4 Å for PDMS (2 CH_3's), 9.3 Å for PEMS (2 CH_2'sand 1 CH_3), and 9.8 Å for PDES (2 CH_2's and 2 CH_3's). The intramolecular structure, characterized by the bond lengths and bond angles, inferred from X-ray scattering were in good agreement with the EA and UA potentials used in the MD simulations and PRISM theory.

The EA model was found to be in very good agreement with experiment over the entire range of wave vectors studied; the UA model was also in very good agreement with experiment at high wave vectors (>6 Å^{-1}). The UA model predicted a somewhat lower height of $H(k)$ for the pronounced peaks near 1 Å for all the siloxanes. PRISM theory was in good agreement with the UA atom simulations for PDMS, PEMS, and PDES. The agreement of PRISM theory with simulation for the siloxanes was about the same as found earlier for polyolefin melts.[27,28]

Blends of siloxanes have been studied[13] with small-angle neutron scattering, and an interesting phase was observed. Future work will focus on MD simulations of binary blends of the three siloxanes studied here.

Acknowledgment. This work was supported by the Division of Materials Sciences, Office of Basic Energy Sciences, U.S. Department of Energy, at the Oak Ridge National Laboratory, managed by UT-Battelle, LLC, for the U.S. Department of Energy under Contract DE-AC05-00OR22725, and at the Sandia National Laboratories, managed by Lockheed Martin Energy Research Corporation, under Contract DE-AC05-840R12400.

References and Notes

(1) Hays, W. R.; Kehrer, G. P.; Monroe, C. M. Presented at the 112th Meeting of the Rubber Division, American Chemical Society, Cleveland, OH, 1977.
(2) Smith, A. L. *Analysis of Silicones, Chemical Analysis*; Wiley: New York, 1974; Vol. 41.
(3) Lynch, W. *Handbook of Silicon Rubber Fabrication*; Van Nostrand Reinhold: New York, 1978.
(4) Meals, R. Silicones. In *Encyclopedia of Chemical Technology*, 2nd ed.; Wiley: New York, 1969; Vol. 18.
(5) Billmeyer, F. W., Jr. *Textbook of Polymer Science*; Wiley-Interscience: New York, 1984.
(6) Mark, J. E. In *Silicon-Based Polymer Science*; Zeigler, J. M., Fearon, F. W. G., Eds.; Advances in Chemistry Series 224; American Chemical Society: Washington, DC, 1990; p 47.
(7) Tobolsky, A. V. *Properties and Structures of Polymers*; Wiley: New York, 1960; p 67.
(8) Sides, S. W.; Curro, J. G.; Grest, G. S.; Stevens, M. J.; Soddemann, T.; Habenschuss, A.; Londono, J. D. *Macromolecules* **2002**, *35*, 6455.
(9) Kim, M. H.; Londono, J. D.; Habenschuss, A. *J. Polym. Sci., Part B: Polym. Phys.* **2000**, *38*, 2480.
(10) Weinhold, J. D.; Curro, J. G.; Habenschuss, A.; Londono, J. D. *Macromolecules* **1999**, *32*, 7276.
(11) Londono, J. D.; Annis, B. K.; Habenschuss, S.; Smith, G. D.; Borodin, O.; Tso, C.; Hsieh, E. T.; Soper, A. K. *J. Chem. Phys.* **1999**, *110*, 8786.
(12) Londono, J. D.; Maranas, J. K.; Mondello, M.; Habenschuss, A.; Grest, G. S.; Graessley, W. W.; Kumar, S. K. *J. Polym. Sci., Part B: Polym. Phys.* **1998**, *36*, 3001. Curro, J. G.; Weinhold, J. D.; Rajasekaran, J. J.; Habenschuss, A.; Londono, J. D.; Honeycutt, J. D. *Macromolecules* **1997**, *30*, 6264.
(13) Yun, S. I.; Melnichenko, Y. B.; Wignall, G. D. *Polymer* **2004**, *45*, 7969.
(14) Cullity, B. D. *Elements of X-ray Diffraction;* Addison-Wesley: Reading, MA, 1956.
(15) Plimpton, S. J. *J. Comput. Phys.* **1995**, *117*, 1 (www.cs.sandia.gov/~sjplimp/lammps.html).
(16) Sun, H. *Macromolecules* **1995**, *28*, 701; *J. Phys. Chem. B* **1998**, *102*, 7338.
(17) Sun, H.; Rigby, D. *Spectrochim. Acta, Part A* **1997**, *53*, 1301.
(18) Frischknecht, A. L.; Curro, J. G. *Macromolecules* **2003**, *36*, 2122.
(19) Hansen, J. P.; McDonald, I. R. *Theory of Simple Liquids*; Academic Press: London, 1986.
(20) Weeks, J. D.; Chandler, D.; Andersen, H. C. *J. Chem. Phys.* **1971**, *54*, 5237.
(21) Makrodimitri, Z. A.; Dohrn, R.; Economou, I. G. *Macromolecules* **2007**, in press.
(22) Schweizer, K. S.; Curro, J. G. *Phys. Rev. Lett.* **1987**, *58*, 246.
(23) Curro, J. G.; Schweizer, K. S. *Macromolecules* **1987**, *20*, 1928.
(24) Curro, J. G.; Schweizer, K. S. *J. Chem. Phys.* **1987**, *87*, 1842.
(25) Chandler, D.; Andersen, H. C. *J. Chem. Phys.* **1972**, *57*, 1930.
(26) Chandler, D. In *Studies in Statistical Mechanics VIII*; Montroll, E. W., Lebowitz, J. L., Eds.; North-Holland: Amsterdam, 1982.
(27) For reviews see: Schweizer, K. S.; Curro, J. G. *Adv. Polym. Sci.* **1994**, *116*, 321. Schweizer, K. S.; Curro, J. G. *Adv. Chem. Phys.* **1997**, *98*, 1. Heine, D.; Grest, G. S.; Curro, J. G. *Adv. Polym. Sci.* **2004**, *176*, 211.
(28) Pütz, M.; Curro, J. G.; Grest, G. S. *J. Chem. Phys.* **2001**, *114*, 2847.
(29) Nath, S. K.; Frischknecht, A. L.; Curro, J. G.; McCoy, J. D. *Macromolecules* **2005**, *38*, 8562.
(30) Flory, P. J. *J. Chem. Phys.* **1949**, *17*, 203.
(31) Chandler, D.; Singh, Y.; Richardson, D. M. *J. Chem. Phys.* **1984**, *91*, 1975.
(32) Nichols, A. L.; Chandler, D.; Singh, Y.; Richardson, D. M. *J. Chem. Phys.* **1984**, *81*, 5109.
(33) Klug, H. P.; Alexander, L. E. *X-ray Diffraction Procedures*, 2nd ed.; Wiley-Interscience: New York, 1974; p 142.
(34) Levy, H. A.; Agron, P. A.; Danford, M. D. *J. Appl. Phys.* **1959**, *30*, 2012.
(35) Narten, A. H.; Levy, H. A. In *Water: A Comprehensive Treatise*; Franks, F., Ed.; Plenum: New York, 1972; Vol. I, p 314.
(36) Cromer, D. T.; Mann, J. B. *J. Chem. Phys.* **1967**, *47*, 1893.
(37) Warren, B. E.; Mozzi, R. L. *Acta Crystallogr.* **1966**, *21*, 459.
(38) *International Tables of X-Ray Crystallography*; Ibers, J. A., Hamilton, W. C., Eds.; Kynoch: Birmingham, 1974; Vol. IV, Chapter 2.2.
(39) Narten, A. H. *J. Chem. Phys.* **1979**, *70*, 299.
(40) *CRC Handbook of Chemistry and Physics*, 75th ed.; Lide, D. R., Ed.; CRC Press: Boca Raton, FL, 1994.
(41) Habenschuss, A.; Narten, A. H. *J. Chem. Phys.* **1990**, *92*, 5692.
(42) Mark, J. E.; Flory, P. J. *J. Am. Chem. Soc.* **1964**, *86*, 138. Flory, P. J.; Crescenzi, V. *J. Am. Chem. Soc.* **1964**, *86*, 146. Mark, J. E.; Erman, E. *Rubberlike Elasticity—A Molecular Primer*; Wiley: New York, 1988. Flory, P. J. *Statistical Mechanics of Chain Molecules*; Interscience: New York, 1969.
(43) Miller, R. L. Crystal Data for Various Polymers. In *Polymer Handbook*, 3rd ed.; Brandrup, J., Immergut, E. H., Eds.; Wiley: New York, 1989; p VI/94.

MA0702290